Determining dominant partial waves in photoproduction via moment analysis

Yannick Wunderlich[1,*]

[1]Universität Bonn, Helmholtz-Institut für Strahlen- und Kernphysik, 53115 Bonn, Germany

Abstract. Important insights into the excitation spectra of baryons are provided by measurements of polarization observables in reactions that involve particles with spin. The photoproduction of a single pseudoscalar meson constitutes an example-reaction that has been under intense investigation recently. We present the basic method of moment-analysis for pseudoscalar meson photoproduction, in which just the angular distributions are analyzed. Using this method, the total angular momentum quantum number of the dominant partial waves contributing in the data can be extracted quickly. Furthermore, the Legendre-coefficients extracted from the angular distributions show interesting composition-patterns in terms of multipoles and allow for instructive comparisons to models. In this contribution, recent results for moment analyses of polarization data for the photoproduction of pions and eta-mesons are shown.

In baryon spectroscopy, the extraction of resonance parameters from scattering data represents the most important central problem. A standard-approach to the solution of this problem, which has taken center stage over the last 50 years, is given by fits of so-called energy-dependent (ED) partial-wave analysis (PWA-) models. Well-known examples for such approaches are the Bonn-Gatchina (BnGa-) model [1], the Jülich-Bonn (JüBo-) model [2, 3], the MAID-analysis [4] and the SAID-PWA [5]. A comprehensive overview of these examples is given in reference [6]. In each case, a reaction-theory is constructed, which satisfies the well-established theoretical S-Matrix principles [7] (analyticity, unitarity and crossing) with varying degrees of rigor. Within the context of such a model, resonances are extracted as poles on the second Riemann-sheet of the scattering amplitude.

Another approach to analyze scattering observables is represented by single-energy (SE) fits, or truncated partial-wave analyses (TPWAs). The simplest possible example is given by $2 \rightarrow 2$-scattering of spinless particles. The only possible observable, i.e. the differential cross section σ_0, is defined in terms of the amplitude as $\sigma_0 = |A(W,\theta)|^2$. The infinite partial-wave series for the amplitude reads

$$A(W,\theta) = \sum_{\ell=0}^{\infty} (2\ell+1) A_\ell P_\ell(\cos\theta). \tag{1}$$

In case one truncates this series at some maximal angular momentum quantum number $\ell_{\max}$, one obtains the following expansion for the cross section (see reference [8])

$$\sigma_0(W,\theta) = \frac{q}{k} \sum_{n=0}^{2\ell_{\max}} a_n^{\sigma_0}(W) P_n(\cos\theta), \tag{2}$$

$$a_n^{\sigma_0}(W) = \sum_{\ell,k=0}^{\ell_{\max}} A_\ell^*(W) C_{\ell k}^n A_k(W). \tag{3}$$

Here, for the scalar example, the coupling-coefficients $C_{\ell k}^n$ in the bilinear equation (3) are well-known and given by [8, 9]

$$C_{\ell k}^n = \langle \ell, 0; k, 0 | n, 0 \rangle^2 \, \frac{(2\ell+1)(2k+1)}{(2n+1)}. \tag{4}$$

Here, the $\langle \ell, m; \ell', m' | n, M \rangle$ are the usual Clebsch-Gordan coefficients.

The central problem in a SE fit is then to *solve* for the real- and imaginary parts of generally phase-constrained[1] partial waves. Thus, one first extracts the Legendre-moments using equation (2). Then, one solves the bilinear equations (3) and it is this second step in which multiple discrete ambiguities [9, 10] can, and probably will, occur. Such ambiguities require additional theoretical input on some subset of the partial waves in order to be resolved. However, one could also remain, in a first instance, with the moment-analysis using (2) and try to use it in order to learn as much about the present dataset as possible.

This latter idea can be generalized to more complicated reactions involving particles with spin without a lot of additional effort. The photoproduction of a single pseudoscalar meson is one example for such a reaction. We write the process in the most general form as $\gamma N \longrightarrow \varphi B$, where φ is a pseudoscalar meson and B a recoil-baryon. The following formalism can thus be applied to the most commonly met example of pion-photoproduction $\varphi B = \pi N$, but also other reactions such as eta-photoproduction $\varphi B = \eta N$ or the production of kaons $\varphi B = K\Lambda, \ldots$ may be studied.

The photoproduction reaction is described using 4

*e-mail: wunderlich@hiskp.uni-bonn.de

[1]Some kind of constraint has to be introduced on the overall phase of the partial waves due to the bilinear nature of the equations (3).

Type	$\check{\Omega}^\alpha$	β_α	γ_α	Type	$\check{\Omega}^\alpha$	β_α	γ_α
	σ_0	0	0		$\check{O}_{x'}$	1	0
$\mathcal{S}$	$\check{\Sigma}$	2	−2	$\mathcal{BR}$	$\check{O}_{z'}$	2	−1
	$\check{T}$	1	−1		$\check{C}_{x'}$	1	0
	$\check{P}$	1	−1		$\check{C}_{z'}$	0	+1
	$\check{E}$	0	0		$\check{T}_{x'}$	2	−1
$\mathcal{BT}$	$\check{G}$	2	−2	$\mathcal{TR}$	$\check{T}_{z'}$	1	0
	$\check{H}$	1	−1		$\check{L}_{x'}$	1	0
	$\check{F}$	1	−1		$\check{L}_{z'}$	0	+1

Table 1: We list here the parameters needed to evaluate the angular parametrizations for the 16 polarization observables of pseudoscalar meson photoproduction given in equations (5) and (6). Such a Table was first published by Tiator [15] (see also references [9, 14]).

complex spin-amplitudes, for instance CGLN-amplitudes $\{F_i(W,\theta), i = 1,\ldots,4\}$ [11], accompanied by 16 polarization observables [12, 13]. The observables are defined in terms of the amplitudes as bilinear hermitean forms and they divide into the subsets of group $\mathcal{S}$ observables $\{\sigma_0, \Sigma, T, P\}$ and furthermore three classes of beam-target ($\mathcal{BT}$), beam-recoil ($\mathcal{BR}$) and target-recoil ($\mathcal{TR}$) observables with four quantities each. The CGLN-amplitudes can be expanded into a well-known partial-wave series using electric and magnetic multipoles $\{E_{\ell\pm}, M_{\ell\pm}\}$ [11, 12].
In case one truncates the multipole-series at some $\ell_{\max}$, the observables acquire the following standard-form [9, 15], which is tantamount to the equations (2,3) in the scalar case:

$$\check{\Omega}^\alpha(W,\theta) = \frac{q}{k} \sum_{n=\beta_\alpha}^{2\ell_{\max}+\beta_\alpha+\gamma_\alpha} (a_{\ell_{\max}})_n^{\check{\Omega}^\alpha}(W)\, P_n^{\beta_\alpha}(\cos\theta), \quad (5)$$

$$(a_{\ell_{\max}})_k^{\check{\Omega}^\alpha}(W) = \langle \mathcal{M}_{\ell_{\max}}(W) \big| C_k^{\check{\Omega}^\alpha} \big| \mathcal{M}_{\ell_{\max}}(W) \rangle . \quad (6)$$

where we have adopted a notation by Chiang and Tabakin [13] to denote the observables $\check{\Omega}^\alpha$ and the index α runs as $\alpha = 1,\ldots,16$. The $P_n^{\beta_\alpha}(\cos\theta)$ are associated Legendre polynomials. The multipoles which are present in a certain truncation-order define the vector

$$\big|\mathcal{M}_{\ell_{\max}}\rangle = [E_{0+}, E_{1+}, M_{1+}, M_{1-}, E_{2+}, E_{2-}, \ldots, M_{\ell_{\max}-}]^T . \quad (7)$$

A set of parameters which defines the photoproduction moment-expansion for all 16 observables is given in Table 1 (cf. reference [14]). Tiator [15] first published similarly formalized expansions for an expansion into powers of $\cos(\theta)$.
The matrices defining the coefficients (6) as bilinear forms are hermitean and have dimensions $(4\ell_{\max}) \times (4\ell_{\max})$, for $\ell_{\max} \geq 1$. We have to report that during the course of the thesis [9], no closed expression for these matrices has been found, which would be analogous to the result (4) from the scalar reactions. However, they can be calculated numerically for each relevant truncation order $\ell_{\max}$. The results for group $\mathcal{S}$ and $\mathcal{BT}$ observables in the order $\ell_{\max} = 5$ have been collected in the appendices of [9]. As an example, the matrix $C_0^{\check{E}}$ is shown in Table 2 for the truncation order $\ell_{\max} = 2$.

It is a fact that once the matrices $C_k^{\check{\Omega}^\alpha}$ are evaluated, one observes that in all cases the matrixes decompose into *blocks* of interference-terms among multipoles of certain definite orbital angular momentum quantum number ℓ. Therefore, we introduce a short-notation [14] for these interference-blocks, using the spectroscopic notation of $S, P, D, \ldots$ for the angular momenta $\ell = 0, 1, 2, \ldots$. For example, a contribution coming from an interference-block

$$\sum_{\mathcal{M},\mathcal{M}'=\{E,M\}} \sum_{p,p'=\{\pm\}} c_{p,p'}^{\mathcal{M},\mathcal{M}'} \mathcal{M}_{0p}^* \mathcal{M}'_{1p'}. \quad (8)$$

between S- and P-wave multipoles would be just written as $\langle S, P\rangle$. Each Legendre-moment generally contains multiple such blocks and therefore, several of the short-forms for interference-blocks are added together in order to describe the partial wave decomposition of a particular moment (see Table 2).
The question whether or not specific minimal subsets of the bilinear forms (6) allow for an unambiguous amplitude extraction in so-called *complete experiments* has been addressed in the classic work by Omelaenko [16] and in the more recent references [9, 17].
The formalism outline above allows for moment-analyses in pseudoscalar meson photoproduction. The following two main aspects are important:

(I) $\ell_{\max}$-analysis: The parametrization (5) of the angular distribution is fitted for different $\ell_{\max}$. The χ^2/ndf is compared for different fits, ascending from the lowest possible order. In case the goodness of fit is unsatisfactory, one has to increase $\ell_{\max}$. Once a good fit is obtained, the resulting $\ell_{\max}$ gives, in a lot of cases, already quite a good estimate for the maximal angular momentum detectable in the data. Plots of χ^2/ndf vs. energy show 'bumps' whenever new important contributions from higher angular momenta enter the data (cf. Figures 3,4, top).

(II) Model-comparisons: The fitted Legendre-moments $(a_{\ell_{\max}})_k^{\check{\Omega}^\alpha}$ can be compared to the right hand side of equation (6), i.e. to the definitions of the moments as bilinear forms in terms of multipoles. The latter can be evaluated using multipoles $\mathcal{M}_\ell$ stemming from an ED model. These comparisons can be performed switching on/off

$$C_0^{\check{E}} = \left[\begin{array}{c|ccc|cccc} 1 & 0 & 0 & 0 & 0 & 0 & 0 & 0 \\ \hline 0 & 3 & 3 & 0 & 0 & 0 & 0 & 0 \\ 0 & 3 & -1 & 0 & 0 & 0 & 0 & 0 \\ 0 & 0 & 0 & 1 & 0 & 0 & 0 & 0 \\ \hline 0 & 0 & 0 & 0 & 6 & 0 & 12 & 0 \\ 0 & 0 & 0 & 0 & 0 & -1 & 0 & -3 \\ 0 & 0 & 0 & 0 & 12 & 0 & -3 & 0 \\ 0 & 0 & 0 & 0 & 0 & -3 & 0 & 3 \end{array}\right] \equiv \langle S, S\rangle + \langle P, P\rangle + \langle D, D\rangle$$

Table 2: The matrix $C_0^{\check{E}}$ which defines the coefficient $(a_2)_0^{\check{E}}$ for an expansion of $\check{E}$ up to $\ell_{\max} = 2$ is shown. Every matrix element defines a particular multipole-interference term. As a generic feature, the matrices $C_n^{\check{\Omega}^\alpha}$ decompose into blocks of interference terms between multipoles with definite orbital angular momentum quantum number ℓ (cf. equations (6) and (7)). Therefore, a short-notation for interference-terms is introduced, using the spectroscopic notation of $S, P, D, \ldots$ for $\ell = 0, 1, 2, \ldots$.

certain model partial waves. In this way, sometimes one obtains valuable information on which partial wave interferences are important. Furthermore, one can try to interpret the results of such comparisons in view of important physical effects visible in the data.

We commence with the discussion of results obtained from new data for π^0- and η-photoproduction [18–20].

In case of π^0-photoproduction, we consider a dataset for the observable $\check{E}$ recently measured by the A2-collaboration at MAMI, and which has been first published in the PhD-thesis [18]. The formula (5) reads, when adapted to the observable $\check{E}$, as follows (see also Table 1)

$$\check{E}(W, \theta) = \frac{q}{k} \sum_{n=0}^{2\ell_{\max}} (a_{\ell_{\max}})_n^{\check{E}}(W)\, P_n(\cos\theta). \qquad (9)$$

This expression has been fitted to the data for different $\ell_{\max}$ and an order of $\ell_{\max} = 4$ was sufficient to yield a satisfactory fit over the whole measured energy-region. The plot of χ^2/ndf vs. energy, as well as several exemplary angular distributions, are shown in Figure 3.

Furthermore, we show plots of the two selected Legendre-moments $a_0^{\check{E}}$ and $a_2^{\check{E}}$ in Figure 1 (see also the thesis [18]). In these plots, the energy-region has been zoomed in, in order to facilitate a more detailed view of the fit-results for the moments. Furthermore, a model-comparison is shown for the Bonn-Gatchina solution BnGa 2017_02, which has been used to re-evaluate both of the moments using different truncation orders. We see that for $a_0^{\check{E}}$ below the $p\eta$-threshold, i.e. for roughly $W < 1500$ MeV, BnGa S- and P-waves are largely sufficient to describe the fit-results for the moment. Very close to the $p\eta$-threshold, a small correction due to D-waves is needed. Then, for all energies above the $p\eta$-threshold, the BnGa F-waves are required to correct the continuous curve such that it coincides with the fitted values for the Legendre-moment. One feature of the shown result is striking: exactly at the $p\eta$-threshold, the fitted values show a pronounces, sudden change in direction, or 'cusp'. Furthermore, analytic S-Matrix theory requires amplitudes to have branch-point singularities precisely at the energies corresponding to the opening of thresholds [7, 21]. Such singularities lead to cusp-like behaviours and they are basically a direct consequence of the combination of the principles of analyticity and unitarity. We conclude that this particular polarization measurement is precise enough to show such sophisticated theoretical effects directly in the data, or more precisely in the extracted Legendre-moments. Furthermore, we see in the comparison-plot that for $a_0^{\check{E}}$, the cusp-effect enters due to a $\langle D, D\rangle$ interference-term.

The same effect can be seen in the plot for $a_2^{\check{E}}$ on the right of Figure 1. The extracted values for the Legendre-moment show a pronounced cusp right at the $p\eta$-threshold. Furthermore, the cusp enters into the BnGa model-curves once the D-waves are included. Here, this cusp-effect is due to the $\langle S, D\rangle$- and $\langle D, D\rangle$ interference-blocks. However, contrary to the results for the moment $a_0^{\check{E}}$, (small) F-wave corrections are important already below the $p\eta$-threshold.

For the process of η-photoproduction, we consider a dataset for the beam-asymmetry $\check{\Sigma}$, which has been recently measured by the CBELSA/TAPS-collaboration [18–20]. When using the general expression (5) for the observable $\check{\Sigma}$, one obtains the following angular parametrization

$$\check{\Sigma}(W, \theta) = \frac{q}{k} \sum_{n=2}^{2\ell_{\max}} (a_{\ell_{\max}})_n^{\check{\Sigma}}(W)\, P_n^2(\cos\theta). \qquad (10)$$

The resulting plots of χ^2/ndf vs. energy, as well as some fitted angular distributions, can be seen in Figure 4. Over the whole fitted energy-region, again a truncation-order of $\ell_{\max} = 4$ is found to yield a satisfactory fit quality.

As an example for an extracted Legendre-moment, we consider here the quantity $a_4^{\check{\Sigma}}$. A plot of the extracted values, as well as a comparison to the Bonn-Gatchina solution BnGa 2014_02, are shown in Figure 2a. The fitted Legendre-moment, which is consistent with zero in the lower energy region, shows a pronounced rise, which looks like a cusp-like structure, right at the $p\eta'$-threshold. Furthermore, the solution BnGa 2014_02 cannot describe this structure. As can be seen in some exemplary angular distributions shown in Figure 2a, the rise of the moment $a_4^{\check{\Sigma}}$ to values significantly larger than zero is in correspondence with the appearance of a backward-peak in the

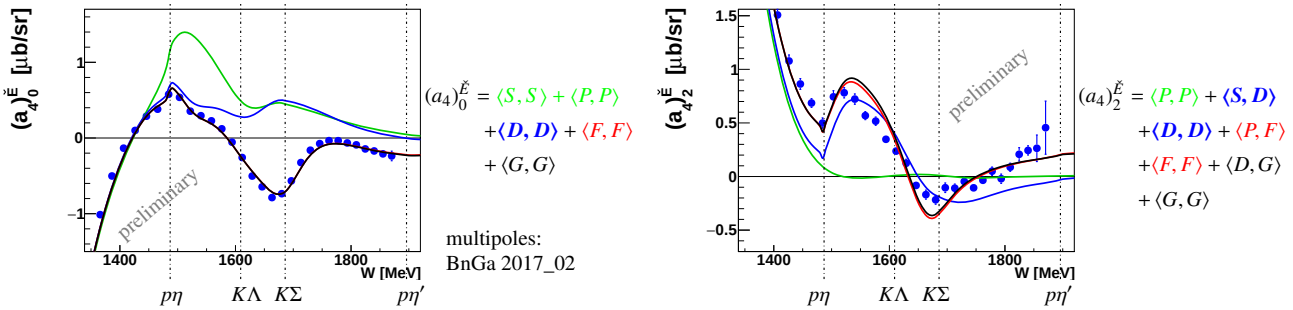

Figure 1: Shown are the two Legendre-moments $a_0^{\check{E}}$ (left) and $a_2^{\check{E}}$ (right), extracted from a recent dataset for the observable $\check{E}$ measured in the reaction $\gamma p \to \pi^0 p$ by the A2-collaboration at MAMI [18]. The coefficients have been extracted using equation (9) in the truncation-order $\ell_{\max} = 4$. The fitted values for the moments are shown as blue dots. Continuous curves show the respective Legendre-moment, evaluated using multipoles from the recent Bonn-Gatchina solution BnGa 2017_02, up to the finite truncation orders: $\ell_{\max} = 1$ (green curve), $\ell_{\max} = 2$ (blue), $\ell_{\max} = 3$ (red) and $\ell_{\max} = 4$ (black). The composition of the respective Legendre moment as a bilinear form in the multipoles is written in the short-notation on the right of the respective plot. Threshold-energies of important photoproduction final-states are illustrated by dash-dotted vertical lines. (color online)

measured angular distribution for $\check{\Sigma}$. This backward-peak needs the modulation $a_4^{\check{\Sigma}} P_4^2(\cos\theta)$ in order to be described. This will be discussed in more detail in upcoming publications (for instance [19]).

For a comparison of the extracted values for the moment $a_4^{\check{\Sigma}}$ to a more recent BnGa-solution, see Figure 2b. There, it is seen that the more recent solution BnGa 2017_02 can describe the cusp a lot better and that furthermore, the cusp-structure enters the model-curve once the G-waves are included, via an $\langle S,G\rangle$ interference-block. For a more involved discussion of the physical meaning of this cusp-effect in η-photoproduction data, see upcoming publications [19].

We conclude that in a new era of polarization-measurements, the precision of the data has become good enough to be directly sensitive to singularities in the amplitudes as dictated by S-matrix theory. This puts new increased demands to the construction and fit of ED models. Furthermore, moment-analysis is the ideal method to make sensitivities to such singularities visible.

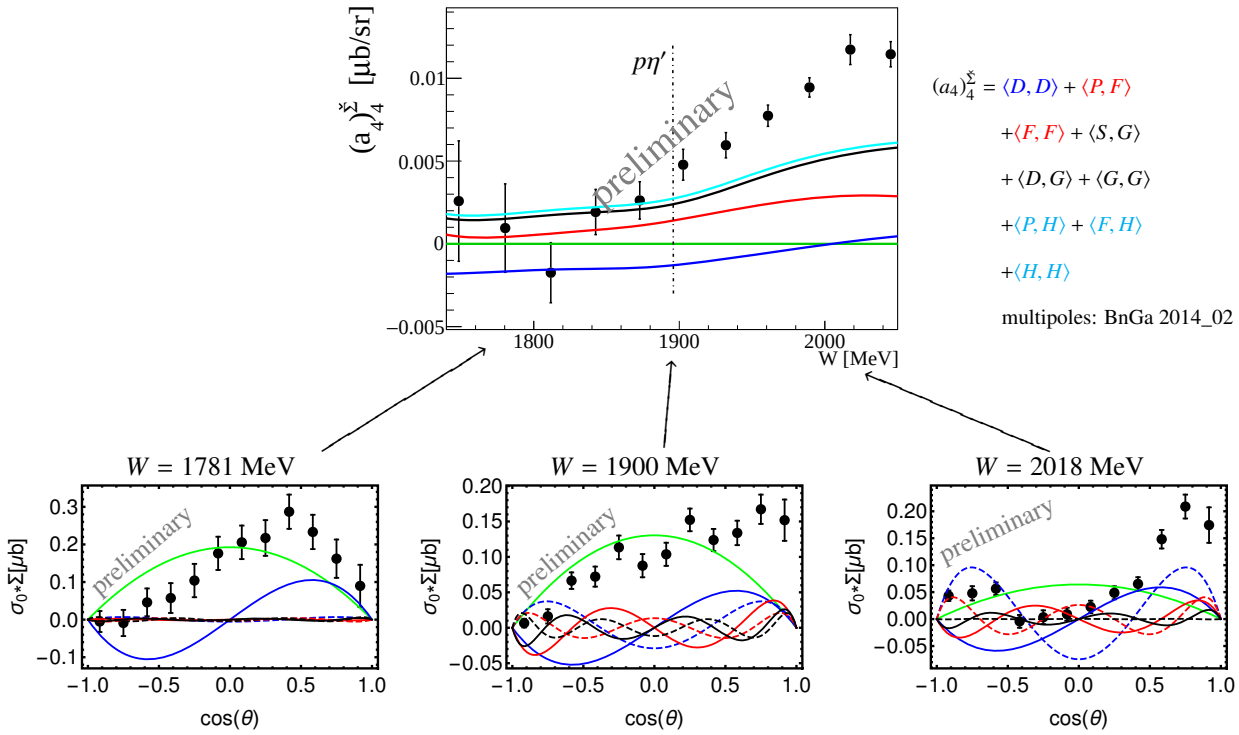

(a) The Legendre-moments $a_4^{\check{\Sigma}}$, extracted from a recent dataset for the observable $\check{\Sigma}$ measured in the reaction $\gamma p \rightarrow \eta p$ by the CBELSA/TAPS-collaboration [18–20] is shown at the top. The coefficient has been extracted using equation (10) in the truncation-order $\ell_{\max} = 4$. The fitted values are shown as black dots. Continuous curves show the Legendre-moment, evaluated using multipoles from the Bonn-Gatchina solution BnGa 2014_02, up to the finite truncation orders: $\ell_{\max} = 1$ (green curve), $\ell_{\max} = 2$ (blue), $\ell_{\max} = 3$ (red), $\ell_{\max} = 4$ (black) and $\ell_{\max} = 5$ (cyan). The composition of the Legendre moment as a bilinear form in the multipoles is written in the short-notation on the right of the plot. The threshold-energy of the $p\eta'$ final state is illustrated by the dash-dotted vertical line. Furthermore, three angular distributions of the profile function $\check{E} = \sigma_0 E$ are shown at the bottom of the figure. For the three exemplary energies, the different contributions from individual Legendre-moments to the fitted function are shown as modulations. In particular, these are the contributions (cf. equation (10)): $a_2^{\check{\Sigma}} P_2^2(\cos\theta)$ (green solid line), $a_3^{\check{\Sigma}} P_3^2(\cos\theta)$ (blue solid line), $a_4^{\check{\Sigma}} P_4^2(\cos\theta)$ (blue dashed line), $a_5^{\check{\Sigma}} P_5^2(\cos\theta)$ (red solid line), $a_6^{\check{\Sigma}} P_6^2(\cos\theta)$ (red dashed line), $a_7^{\check{\Sigma}} P_7^2(\cos\theta)$ (black solid line), $a_8^{\check{\Sigma}} P_8^2(\cos\theta)$ (black dashed line). Arrows indicate the corresponding energy-bins in the plot of $a_4^{\check{\Sigma}}$. (color online)

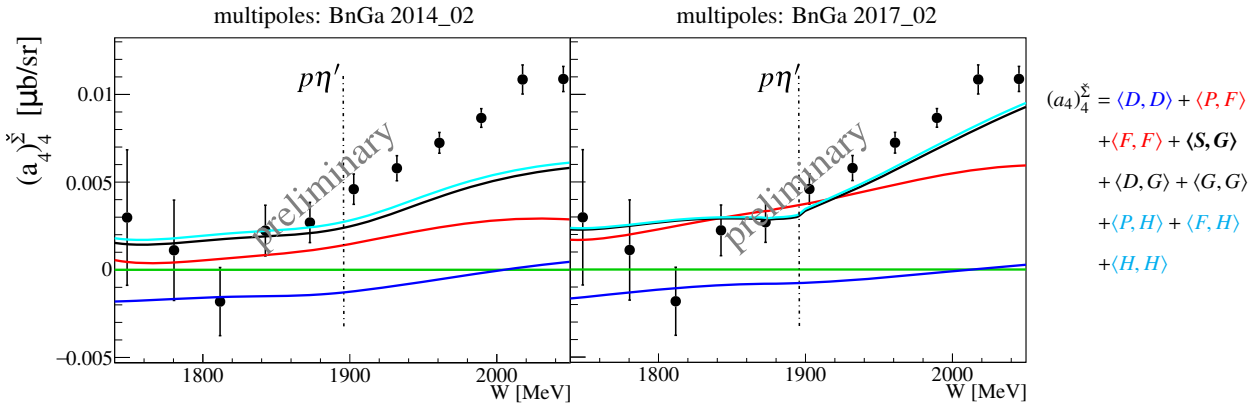

(b) Here, the same Legendre-moment is shown as in Figure 2a (see also references [18, 19]). However, for the two plots different BnGa-solutions were used in order to evaluate the continuous curves, i.e. the solutions BnGa 2014_02 (left) and BnGa 2017_02 (right). In particular, in case of BnGa 2017_02, one can see the $p\eta'$-cusp in the continuous curves once the G-waves are included. The composition of the Legendre-moment in terms of the short-notations for interference terms is shown on the right of the plots. The threshold-energy of the $p\eta'$ final state is shown as a dash-dotted vertical line. (color online)

Figure 2: Plots showing the Legendre-moment $a_4^{\check{\Sigma}}$, extracted from η-photoproduction data [18–20].

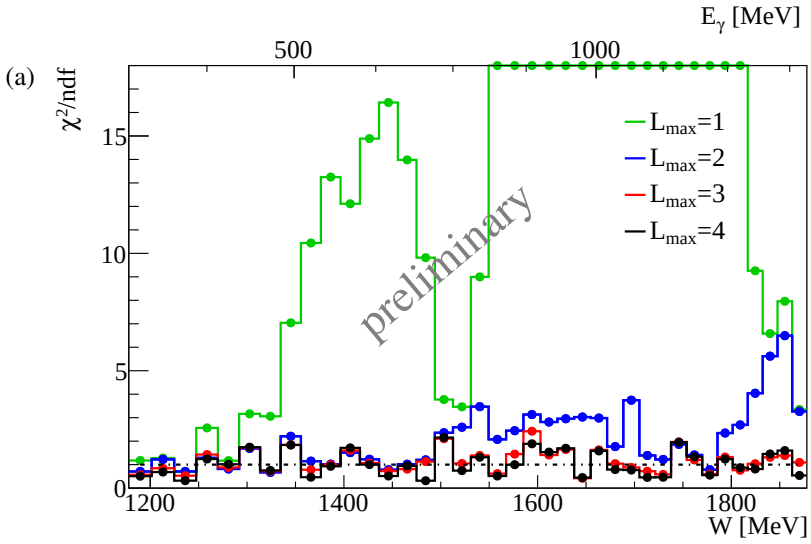

Figure 3: The double-polarization observable $\check{E}$ data from the A2-collaboration at MAMI [18], with only statistical error, was fitted using associated Legendre polynomials according to the Legendre moment expansions (5,9) and truncating the expansion at $\ell_{max} = 1, \ldots, 4$. (a) The resulting χ^2/ndf values for fits with different orders ℓ_{max} as a function of the center of mass energy W and photon LAB-energy E_γ are shown. (b) 12 out of 38 selected angular distributions of $\check{\Sigma}$ (black points) are plotted together with fit-curves for different ℓ_{max} (solid lines), starting at W= 1484 MeV up to 1855 MeV. (color online)

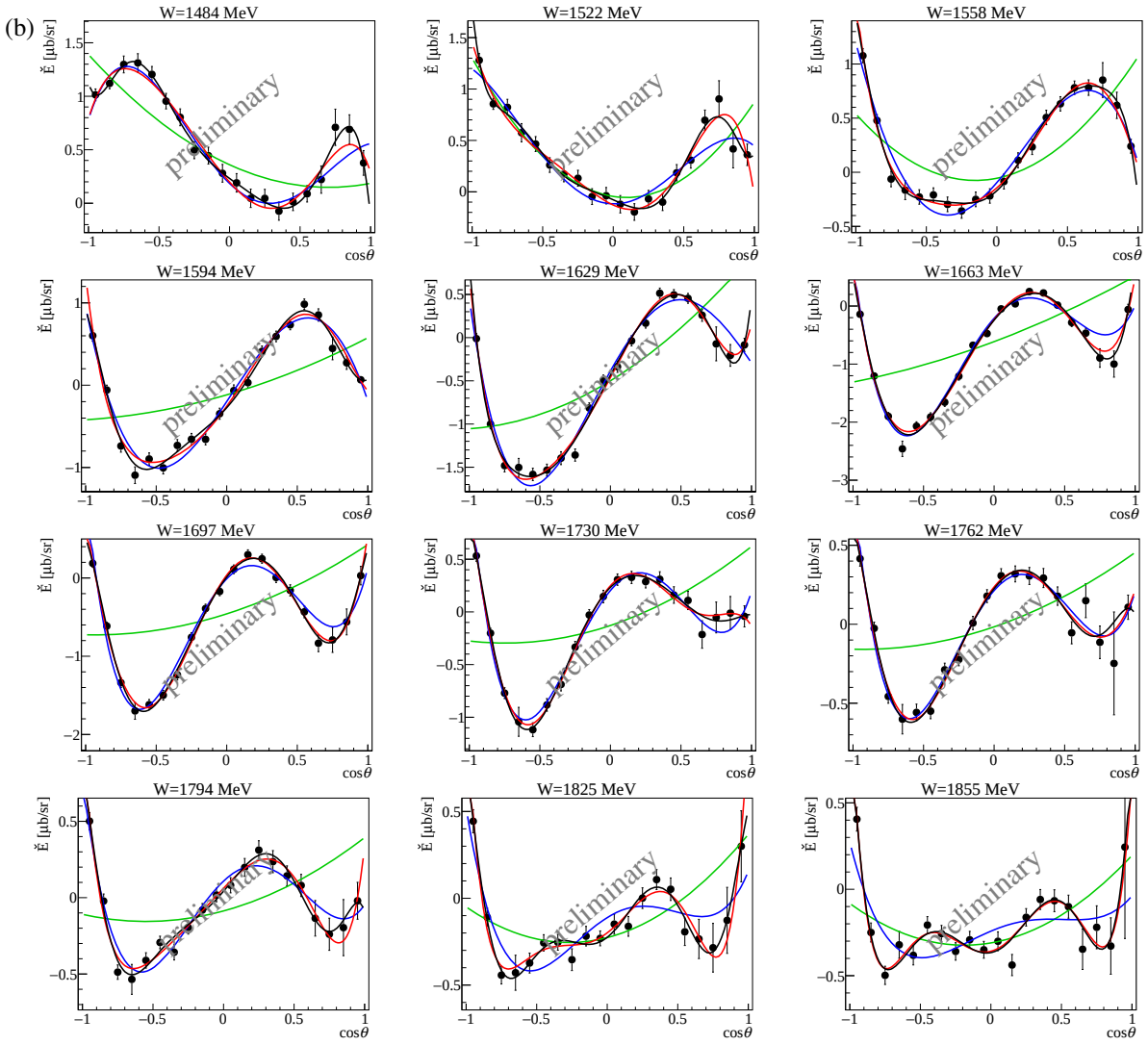

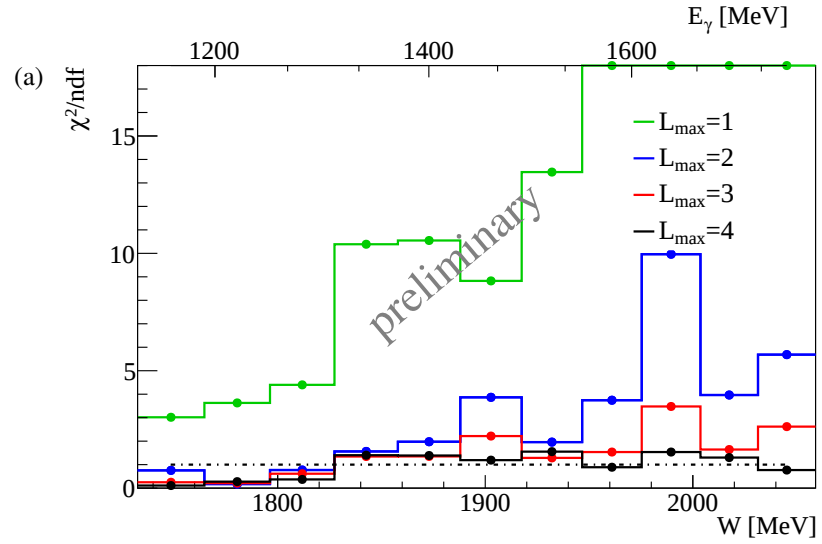

Figure 4: The beam-asymmetry $\check{\Sigma}$ data from the CBELSA/TAPS-collaboration [18, 19], with only statistical error, was fitted using the expansion into Legendre moments given in equations (5,10) and truncating the expansion at $\ell_{max} = 1, \ldots, 4$. (a) The resulting χ^2/ndf values for fits with different orders ℓ_{max} as a function of the center of mass energy W and photon LAB-energy E_γ are shown. (b) 6 out of 11 selected angular distributions of $\check{\Sigma}$ (black points) are plotted together with curves corresponding to fits with different ℓ_{max} (solid lines), starting at W= 1748 MeV up to 2045 MeV. (color online)

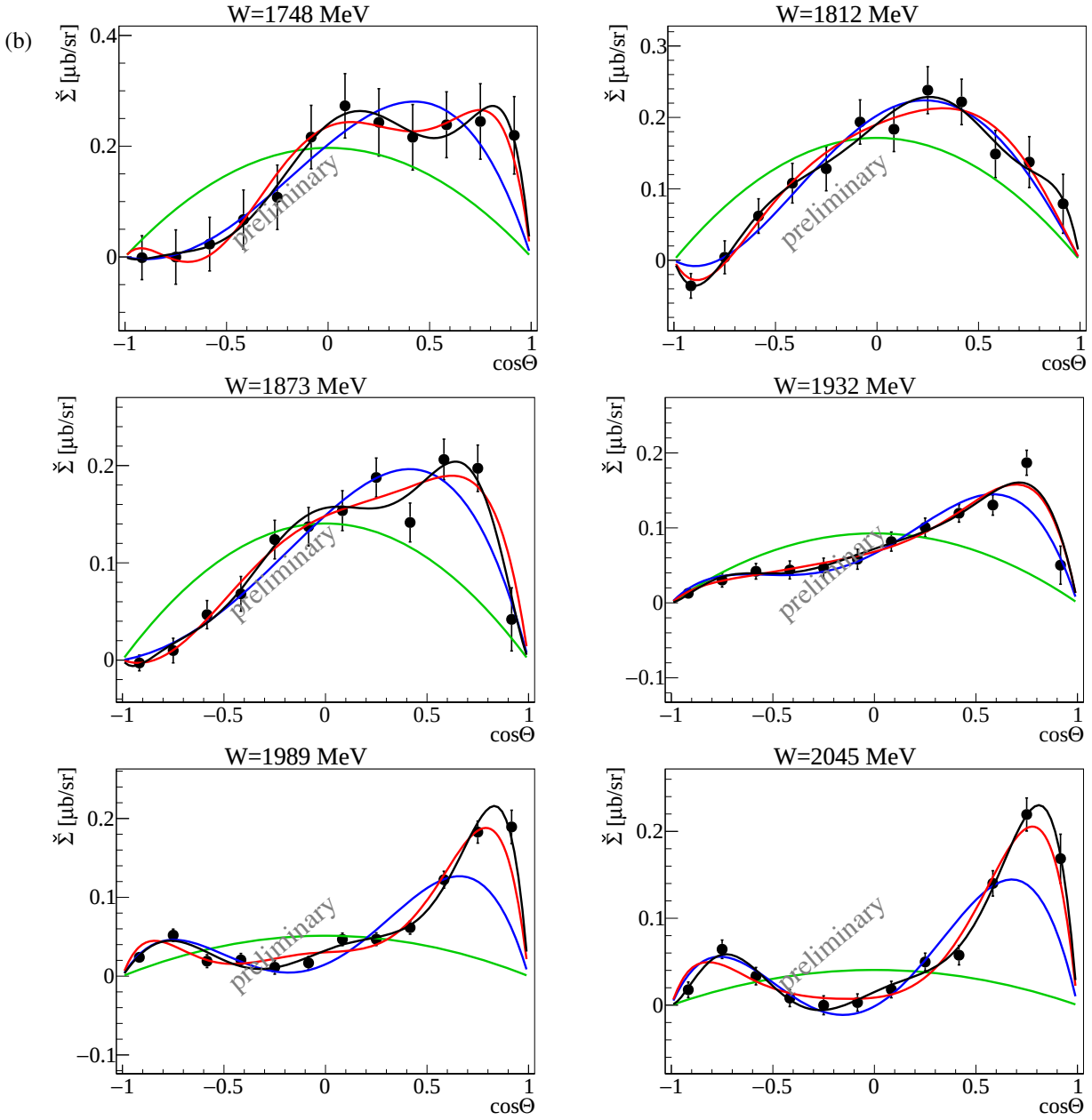

References

[1] A. V. Anisovich, R. Beck, E. Klempt, V. A. Nikonov, A. V. Sarantsev and U. Thoma, Eur. Phys. J. A **48**, 15 (2012).

[2] D. Ronchen *et al.*, Eur. Phys. J. A **49**, 44 (2013) doi:10.1140/epja/i2013-13044-5 [arXiv:1211.6998 [nucl-th]].

[3] M. Doring, C. Hanhart, F. Huang, S. Krewald and U.-G. Meißner, Phys. Lett. B **681**, 26 (2009) doi:10.1016/j.physletb.2009.09.052 [arXiv:0903.1781 [nucl-th]].

[4] D. Drechsel, S. S. Kamalov and L. Tiator, Eur. Phys. J. A **34**, 69 (2007).

[5] R. A. Arndt, W. J. Briscoe, I. I. Strakovsky and R. L. Workman, Phys. Rev. C **74**, 045205 (2006).

[6] A. V. Anisovich *et al.*, Eur. Phys. J. A **52**, no. 9, 284 (2016) doi:10.1140/epja/i2016-16284-9 [arXiv:1604.05704 [nucl-th]].

[7] R. J. Eden, P. V. Landshoff, D. I. Olive and J. C. Polkinghorne, "The analytic S-matrix", Cambridge University Press, (1966).

[8] J. E. Bowcock and H. Burkhardt, Rep. Prog. Phys. **38**, 1099 (1975).

[9] Y. Wunderlich, "The complete experiment problem of pseudoscalar meson photoproduction in a truncated partial wave analysis", url: http://hss.ulb.uni-bonn.de/2019/5353/5353.htm, PhD-thesis, University of Bonn (2019).

[10] A. Gersten, Nucl. Phys. B **12**, p. 537 (1969).

[11] G. F. Chew, M. L. Goldberger, F. E. Low, and Y. Nambu, Phys. Rev. **106**, 1345 (1957).

[12] A. M. Sandorfi, S. Hoblit, H. Kamano, T. -S. H. Lee, J. Phys. G **38**, 053001 (2011).

[13] W.-T. Chiang and F. Tabakin, Phys. Rev. C **55**, 2054 (1997).

[14] Y. Wunderlich, F. Afzal, A. Thiel and R. Beck, Eur. Phys. J. A **53**, no. 5, 86 (2017).

[15] L. Tiator, AIP Conf. Proc. **1432**, 162 (2012).

[16] A. S. Omelaenko, Sov. J. Nucl. Phys. **34**, 406 (1981).

[17] Y. Wunderlich, R. Beck and L. Tiator, Phys. Rev. C **85**, 055203 (2014).

[18] F. Afzal, "Measurement of the beam and helicity asymmetries in the reactions $\gamma p \to p\pi^0$ and $\gamma p \to p\eta$", url: http://hss.ulb.uni-bonn.de/2019/5551/5551.htm, PhD-thesis, University of Bonn (2019).

[19] F. Afzal *et al.*, "Precise beam asymmetry Σ data for $\gamma p \to \eta p$ in the $p\eta'$ threshold region", in preparation (2019).

[20] F. Afzal [CBELSA/TAPS Collaboration], "Recent results from the CBELSA/TAPS experiment at ELSA", contribution to *NSTAR2019* (2019).

[21] S. Ceci, M. Doring, C. Hanhart, S. Krewald, U.-G. Meissner and A. Svarc, Phys. Rev. C **84**, 015205 (2011).